energies

MDPI

Article

Research on the Volumetric Efficiency of 2D Piston Pumps with a Balanced Force

Yu Huang, Jian Ruan *, Yong Chen, Chuan Ding and Sheng Li

Key Laboratory of Special Purpose Equipment and Advanced Manufacturing Technology, Ministry of Education & Zhejiang Province, Zhejiang University of Technology, Hangzhou 310014, China; YuHuang1117@outlook.com (Y.H.); yongchen95@outlook.com (Y.C.); chuanding@zjut.edu.cn (C.D.); ShengLi_zjut@outlook.com (S.L.)

* Correspondence: ruanjiane@zjut.edu.cn

Received: 15 July 2020; Accepted: 2 September 2020; Published: 14 September 2020



Abstract: Axial piston pumps with high rotational speeds are required in many fields to increase the power-to-weight ratio. However, three main sliding friction pairs in the pump restrict the increase in rotational speed. To solve this problem, we propose a 2D piston pump with a balanced force that contains a sliding friction pair. Firstly, the mechanical structure and working principle of the pump are described. Then, the pump volumetric efficiency is studied by mathematical modeling, and volumetric losses containing backflow and leakage are analyzed and discussed from the perspectives of load pressure and rotational speed. A test bench that verifies the mathematical model is built to measure the volumetric efficiency of the tested pump. We have found that the increase in rotational speed can help to increase the pump volumetric efficiency, and the mathematical model is consistent with the tested data for 1000 rpm but demonstrates a remarkable difference from the tested data for 3000 rpm. Thus, the temperature field of the pump and the viscosity-temperature characteristics of the oil must be taken into account to increase volumetric efficiency further.

Keywords: 2D piston pump; backflow; leakage; volumetric losses

1. Introduction

Hydraulic systems are widely used in many fields because of their high power density, quick dynamic response, and strong load capacity [1–3]. In recent years, due to their high power-to-weight ratio, electro-hydrostatic actuator (EHA)-installed axial piston pumps as the oil source are used to replace the centrifugal hydraulic system, which uses centrifugal pumps as the oil source in the aerospace industry [4].

A high power density is the most important requirement for axial piston pumps used in the aerospace industry, and the power-to-weight ratio of energy components needs to be further improved [5]. This is often achieved by increasing rotational speed [6]. The displacements of axial piston pumps of various manufacturers at various rotational speeds are shown in Figure 1. In aerospace applications, the rotational speed of the axial piston pump is required to be greater than 10,000 rpm [7]. When the rotational speed exceeds 10,000 rpm, as shown in Figure 1, the pump displacement decreases to less than 5 mL/r. Increasing the rotational speed and reducing the displacement of the pump can increase the power density, known as the "reduction effect". This reduction effect is significant for low rotational speed pumps, but it becomes less noticeable when the rotational speed exceeds 10,000 rpm [6].

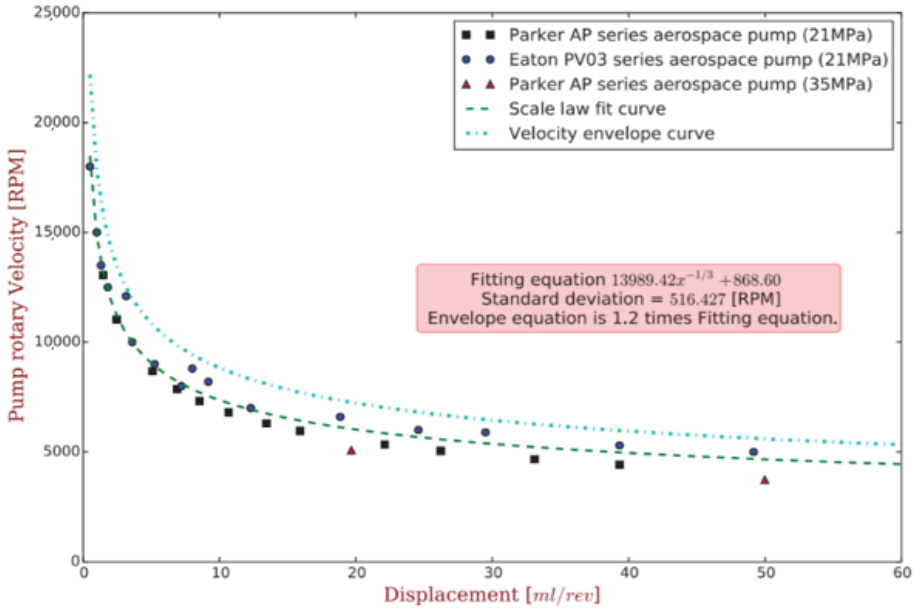


Figure 1. Displacements of axial piston pumps of various manufacturers at different rotational speeds [8].

On the other hand, the rotational speed of axial piston pumps is limited by two factors in practical applications [9]. The first one is the presence of three main sliding friction pairs in axial piston pumps [10–12]. The friction pairs subjected to overturning moments generate mechanical losses during rotation [13]. Especially at high speeds, the rise of the overturning torque causes direct metal-to-metal contact between the sliding surfaces in the three main lubrication surfaces [14]. This problem can be improved to a certain extent by coating on the surface of these friction pairs [15]. The second factor that limits the rotational speed is the thermal problem. The combination of small displacement and high speed generates heat and reduces the heat dissipation capacity of the axial piston pump [16,17]. In addition, the churning losses are generated by the rotating parts and increase the oil temperature at high rotational speeds [18–20].

Ruan group has proposed a new type of axial piston pump based on a "two-dimensional" concept, named 2D piston pump [21–23]. As shown in Figure 2, through the cooperation of the rollers and guiding rails, the rotation of the 2D piston is converted into the reciprocation, thereby achieving sucking and discharging oil. The 2D piston pump has only a sliding friction pair between the 2D piston and cylinder block, and the radial force of the 2D piston is balanced and is not affected by the overturning torque [24]. Thus, the 2D piston pump has the potential to achieve high rotational speed.

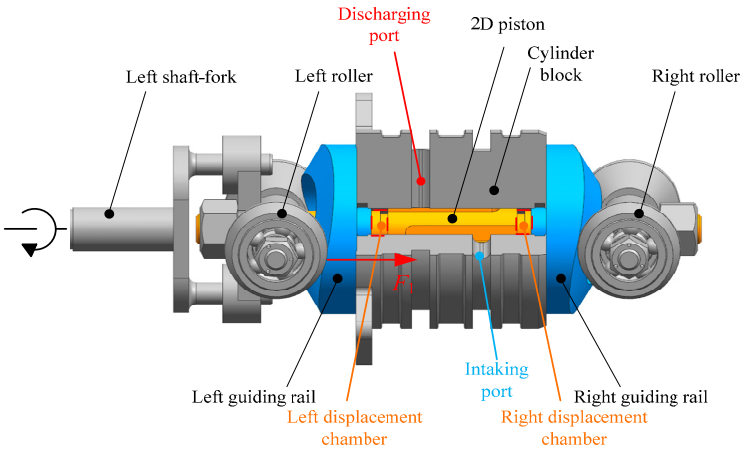


Figure 2. State of the traditional 2D piston pump at the left displacement chamber discharging oil.

However, vibration is generated by the pump at high rotational speeds. When the 2D piston rotates, the cylinder block is moved by a force F_1, which is generated by the rollers. The force acts on the left side of the cylinder block at the left displacement chamber discharging oil, and the force acts on the right side of the cylinder block at the right displacement chamber discharging oil. Due to the traditional 2D pump designed to discharge oil alternately between the left and right displacement chambers, the cylinder block is moved by an alternate force and generates vibration [25].

To solve this problem, we propose a 2D piston pump with a balanced force using a well-balanced force. By adding a balancing set, the cylinder block is subjected to a pair of balanced forces, thereby eliminating the vibration [26]. Firstly, the mechanical structure and working principle of the proposed piston pump are described in Section 2. Then, the volumetric efficiency of the pump is researched through mathematical modeling in Section 3. The pump volumetric losses are analyzed and discussed from the perspectives of load pressure and rotational speed in Section 4. Finally, a test bench is built to measure the volumetric efficiency of the pump and verify the mathematical model.

2. Mechanical Structure and Working Principle of the 2D Piston Pump with a Balanced Force

As shown in Figure 3a, the 2D piston pump with a balanced force consists of successively, from left to the right, a fork shaft, left roller set, left guiding rail, cylinder block, 2D piston, pump shell, right guiding rail, right roller set, and right fork. The roller sets are divided into driving rollers and balancing rollers. As shown in Figure 3b,c, the orange rollers are the driving rollers, and the blue rollers are the balancing rollers. The driving rollers are fixed to the 2D piston, and the balancing rollers are fixed to the piston ring. The two sets are combined and have a phase difference of 90 deg between them in the circumferential direction through the two forks, whereas they have relatively independent axial motions. The 2D piston is hollow to install the transmission shaft, and it is precisely contained with the cylinder block.

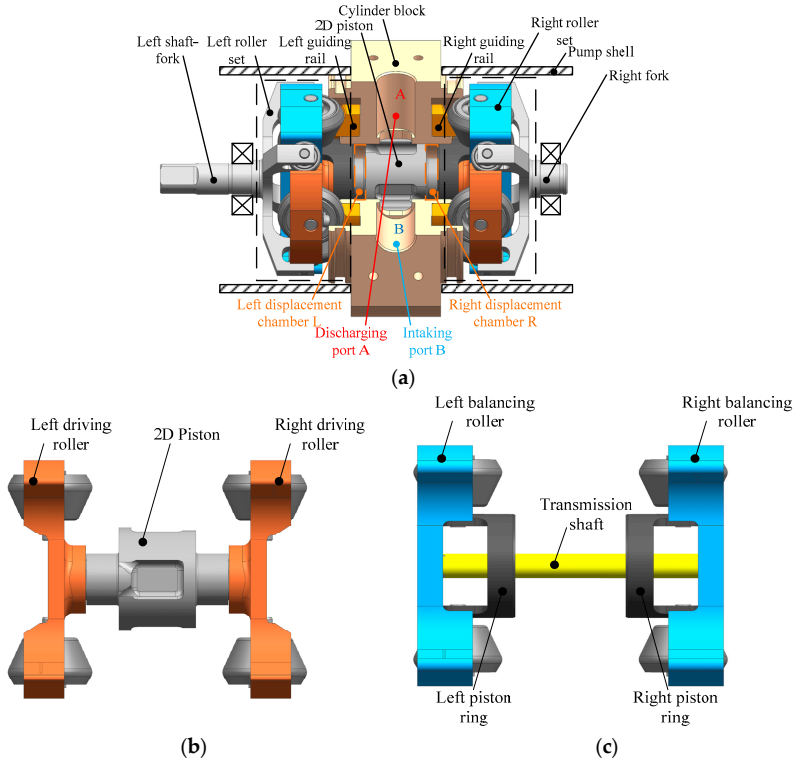


Figure 3. Configuration of the 2D piston pump with a balanced force and its two critical active parts [18]: (**a**) the overview sight; (**b**) the driving set; and (**c**) the balancing set.

The left and right displacement chambers, both having the same working principle, are composed of the 2D piston, piston rings, and cylinder block, but have a phase difference of 90 deg. Taking the left displacement chamber as an example, the working principle of oil suction and discharge is introduced.

The pump's state described in Figure 4a is assumed to be zero at the initial state, where the left displacement chamber is at the maximum volume and prepares to discharge oil. From Figure 4a–c, the 2D piston rotates from 0 deg to 90 deg. The left displacement chamber is compressed from the maximum, causing the oil to be discharged into the discharging port out of the left displacement chamber. From Figure 4a–c, the 2D piston rotates from 90 deg to 180 deg. The left displacement chamber expands from the minimum, causing the oil to be sucked from the intaking port into the left displacement chamber.

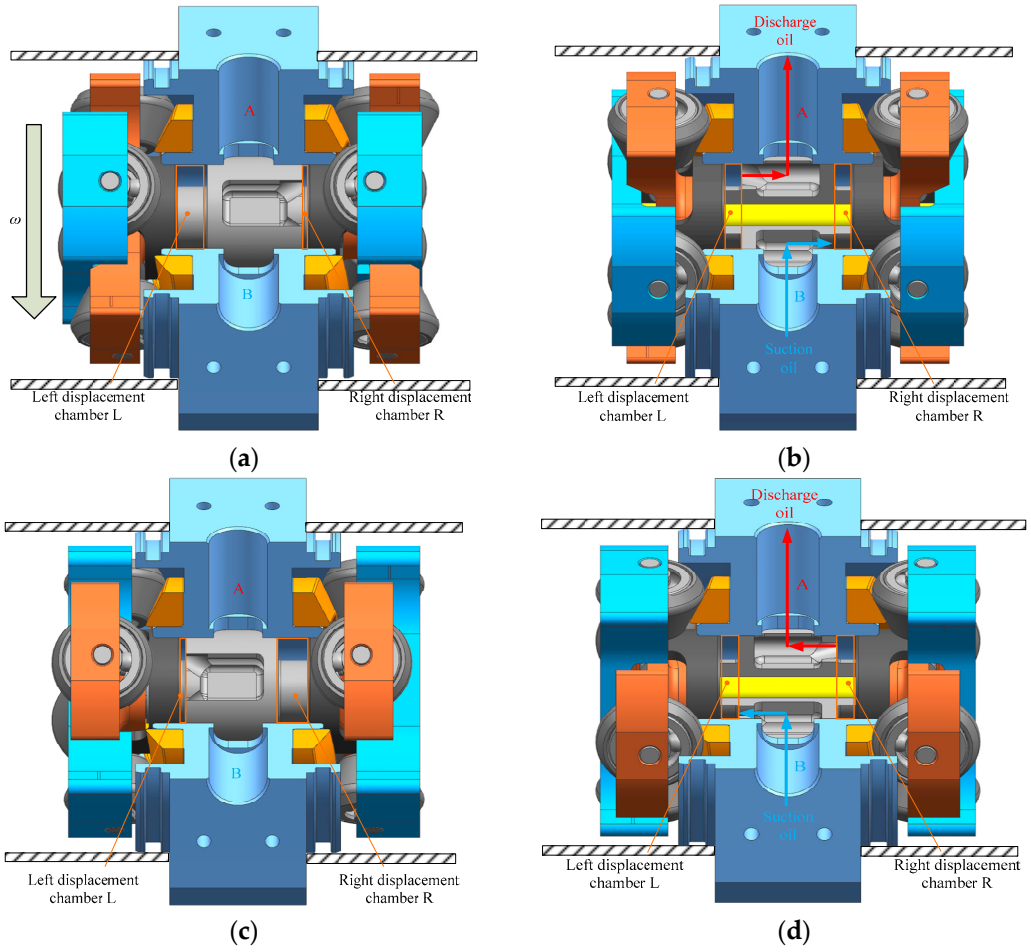


Figure 4. A working period of the 2D piston pump with a balanced force [18]: (**a**) at the initial point of rotation, (**b**) at a rotational angle of 45 deg, (**c**) at a rotational angle of 90 deg, (**d**) at a rotational angle of 135 deg.

As soon as the left shaft-fork is rotated by a motor, both the driving and balancing sets are rotated at the same pace. When the rollers rotate under the constraint of the guiding rails, the rotation of the sets is transformed into the relative reciprocating motion. As shown in Figure 5, when the rollers rotate from 0 deg to 45 deg, the driving set moves left with uniform acceleration, and the balancing set moves right with a uniform acceleration, decreasing the volume of the left displacement chamber and increasing that of the right displacement chamber. Therefore, the force acting on the cylinder block by the driving set can be balanced by force from the balancing set.

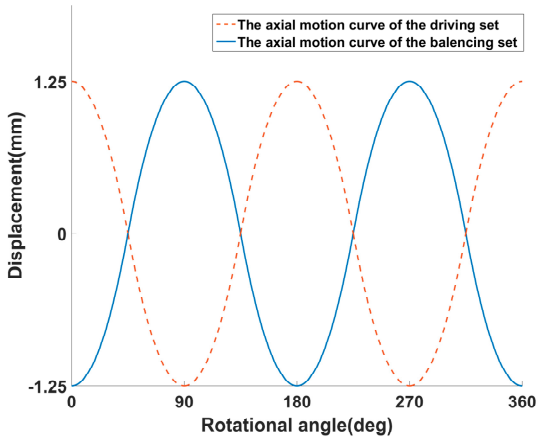


Figure 5. The axial motions of the driving and balancing sets.

3. Mathematical Modeling

Since the working principle of the left displacement chamber is consistent with that of the right displacement chamber, the left displacement chamber is taken as an example to model its volumetric efficiency. As shown in Figures 4a and 6, the rotational degree is assumed to be zero at the initial moment, where the left displacement chamber is at the maximum volume and starts to discharge oil. Assuming the oil in the left displacement chamber is compressible, the instantaneous left displacement chamber pressure is governed by the following pressure build-up Equation (1)

$$\frac{dp_{\mathrm{L}}}{dt} = \beta_{\mathrm{e}} \frac{(\frac{dV_{\mathrm{L}}}{dt} + Q_{\mathrm{o}} + Q_{\mathrm{i}} + Q_{\mathrm{L}})}{V_{\mathrm{L}}} \tag{1}$$

where p_{L} is the instantaneous left displacement chamber pressure, t is the rotating time from 0 deg, β_{e} is the bulk modulus of the oil, V_{L} is the instantaneous left displacement chamber volume, Q_{o} is the outlet flow of the left displacement chamber, Q_{i} is the inlet flow of the left displacement chamber, and Q_{L} is the leakage flow of the left displacement chamber. The instantaneous left displacement chamber volume is determined by the positions of the left piston ring and 2D piston, where their motions are accorded to uniform acceleration and deceleration [24]. The left piston ring velocity v_{pr} and the left 2D piston velocity v_{p} are described by Equation (2).

$$v_{\mathrm{pr}} = -v_{\mathrm{p}} = \begin{cases} at & 0 < t \le \frac{\pi}{4\omega} \\ a(\frac{\pi}{2\omega} - t) & \frac{\pi}{4\omega} < t \le \frac{3\pi}{4\omega} \\ a(t - \frac{\pi}{\omega}) & \frac{3\pi}{4\omega} < t \le \frac{\pi}{\omega} \end{cases} \tag{2}$$

where a is the acceleration and decided by the rotational speed n and the 2D piston stroke L_{s} that is consistent with the left piston ring stroke, and ω is the rotational angular velocity. When the pump rotates from 0 deg to 45 deg, the 2D piston moves left with uniform acceleration, and the axial displacement is half of the 2D piston stroke. The acceleration is calculated by Equation (3).

$$a = \frac{L_{\mathrm{s}}}{(t_{45\mathrm{deg}})^2} = \frac{16\omega^2 L_{\mathrm{s}}}{\pi^2} \tag{3}$$

where t_{45deg} is the rotating time from 0 deg to 45 deg. Integrating the left piston ring velocity and 2D piston velocity, the instantaneous left displacement chamber volume is calculated by Equation (4).

$$V_L = \begin{cases} V_M - 2A \cdot \frac{1}{2} a t^2 & 0 < t \le \frac{\pi}{4\omega} \\ V_M - Aa\frac{\pi^2}{8\omega^2} + 2A \cdot \frac{1}{2} a (\frac{\pi}{2\omega} - t)^2 & \frac{\pi}{4\omega} < t \le \frac{\pi}{2\omega} \\ V_M - Aa\frac{\pi^2}{8\omega^2} + 2A \cdot \frac{1}{2} a (t - \frac{\pi}{2\omega})^2 & \frac{\pi}{2\omega} < t \le \frac{3\pi}{4\omega} \\ V_M - 2A \cdot \frac{1}{2} a (t - \frac{\pi}{\omega})^2 & \frac{3\pi}{4\omega} < t \le \frac{\pi}{\omega} \end{cases} \quad (4)$$

where V_M is the maximum volume of the left displacement chamber. Equation (5) is obtained by differentiating Equation (4).

$$\frac{dV_L}{dt} = \begin{cases} -2Aat & 0 < t \le \frac{\pi}{4\omega} \\ -2Aa(\frac{\pi}{2\omega} - t) & \frac{\pi}{4\omega} < t \le \frac{3\pi}{4\omega} \\ -2Aa(t - \frac{\pi}{\omega}) & \frac{3\pi}{4\omega} < t \le \frac{\pi}{\omega} \end{cases} \quad (5)$$

The outlet flow and the inlet flow can be calculated by using the standard orifice Equations (6) and (7).

$$Q_o = C_d A_{out} \sqrt{\frac{2|p_L - p_{Load}|}{\rho}} \text{sign}(p_L - p_{Load}) \quad (6)$$

$$Q_i = C_d A_{in} \sqrt{\frac{2|p_T - p_L|}{\rho}} \text{sign}(p_L - p_T) \quad (7)$$

where C_d is the orifice coefficient, A_{out} and A_{in} are the open areas of the discharging ports and intaking ports, respectively, p_{Load} and p_T are the pressures of the load and tank, respectively, and ρ is the oil density.

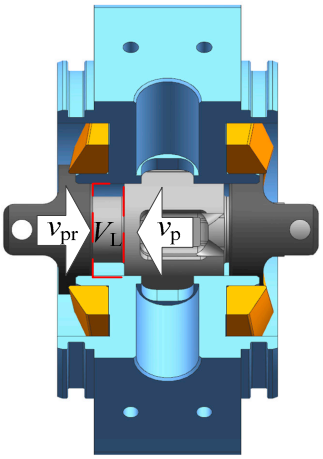


Figure 6. The maximum volume of the left displacement chamber.

By expanding the outer circle of the 2D piston into a plane, as shown in Figure 7, when the pump rotates from 0 deg to 90 deg, the state that the left displacement chamber connects with the discharging ports can be described in detail. Because the rotational speed and port length L_g are constant, when the rotational angle is from 0 deg to 45 deg, the open area increases linearly; when the rotational angle is

from 45 degrees to 90 degrees, the open area decreases linearly. The open areas of the discharging ports and intaking ports can be calculated by Equations (8) and (9) [23]

$$A_{\text{out}} = \begin{cases} 2\frac{D\omega}{2}t \cdot L_{\text{g}} & 0 < t \le \frac{\pi}{4\omega} \\ 2\frac{D\pi}{8}L_{\text{g}} - 2\frac{D\omega}{2}(t - \frac{\pi}{4\omega}) \cdot L_{\text{g}} & \frac{\pi}{4\omega} < t \le \frac{\pi}{2\omega} \\ 0 & \frac{\pi}{2\omega} < t \le \frac{\pi}{\omega} \end{cases} \tag{8}$$

$$A_{\text{in}} = \begin{cases} 0 & 0 < t \le \frac{\pi}{2\omega} \\ 2\frac{D\omega}{2}(t - \frac{\pi}{2\omega}) \cdot L_{\text{g}} & \frac{\pi}{2\omega} < t \le \frac{3\pi}{4\omega} \\ 2\frac{D\pi}{8} \cdot L_{\text{g}} - 2\frac{D\omega}{2}(t - \frac{3\pi}{4\omega}) \cdot L_{\text{g}} & \frac{3\pi}{4\omega} < t \le \frac{\pi}{\omega} \end{cases} \tag{9}$$

where D is the 2D piston diameter.

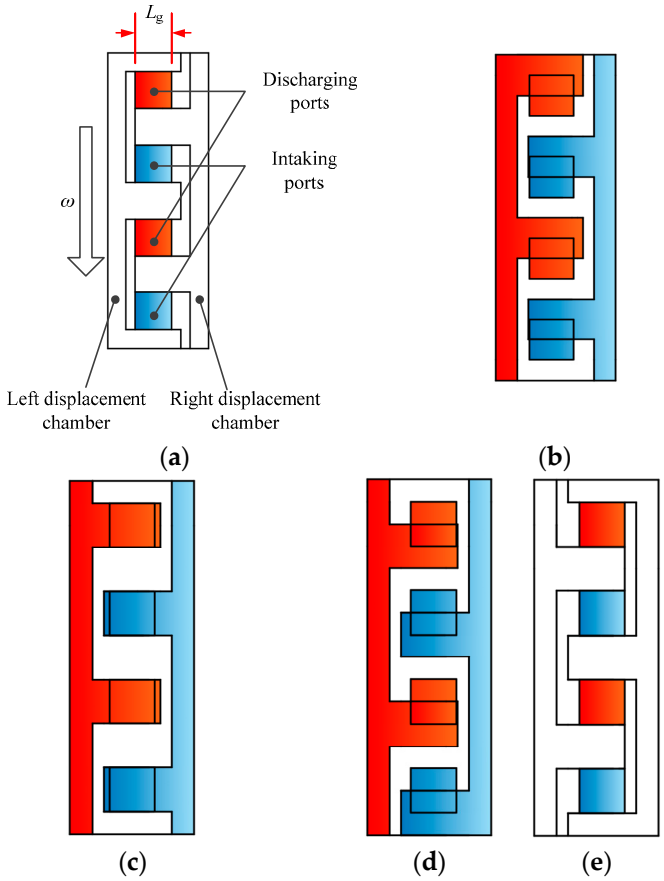


Figure 7. The open areas of the discharging and intaking ports at various rotational angles: (**a**) 0 deg; (**b**) 22.5 deg; (**c**) 45 deg; (**d**) 67.5 deg; (**e**) 90 deg.

The leakage flow consists of the external leakage flow Q_{oL} and the internal leakage flow Q_{iL}.

Due to the clearances h between the piston rings, 2D piston, and cylinder block, as shown in Figure 8, the external leakage flow can be calculated using the standard leakage Equation (10).

$$Q_{\text{oL}} = \pi D \cdot \left(\frac{1}{12\mu L\text{pr}} h^3 \cdot (p_{\text{L}} - p_{\text{T}}) - \frac{h}{2} v_{\text{pr}}\right) + \pi d \cdot \frac{1}{12\mu \cdot [2(L_{\text{pr}} - L_{\text{D}}) + L_{\text{D}}]} h^3 \cdot (p_{\text{L}} - p_{\text{T}}) \tag{10}$$

where μ is the oil dynamic viscosity, L_{pr} is the contact length between the left piston ring and cylinder block, d is the small diameter of the 2D piston, L_{D} is the minimum contact length between the left piston ring and cylinder block and the left piston ring and the 2D piston. Since the motions of the 2D

piston and left piston ring are relative, the external leakage between the left piston ring and 2D piston generated by the velocity is not considered. The length between the left piston ring and the cylinder block is calculated by integrating Equation (2) [22].

$$L_{\mathrm{pr}} = \begin{cases} L_{\mathrm{D}} + \frac{1}{2}at^2 & 0 < t \le \frac{\pi}{4\omega} \\ L_{\mathrm{D}} + a\frac{\pi^2}{16\omega^2} - \frac{1}{2}a(\frac{\pi}{2\omega} - t)^2 & \frac{\pi}{4\omega} < t \le \frac{\pi}{2\omega} \\ L_{\mathrm{D}} + a\frac{\pi^2}{16\omega^2} - \frac{1}{2}a(t - \frac{\pi}{2\omega})^2 & \frac{\pi}{2\omega} < t \le \frac{3\pi}{4\omega} \\ L_{\mathrm{D}} + \frac{1}{2}a(\frac{\pi}{\omega} - t)^2 & \frac{3\pi}{4\omega} < t \le \frac{\pi}{\omega} \end{cases} \tag{11}$$

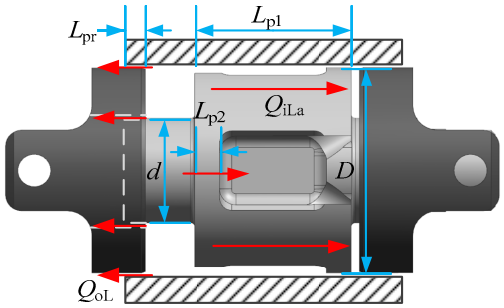


Figure 8. The external leakage and the internal axial leakage.

The internal leakage flow is also composed of two parts: the internal axial leakage flow Q_{iLa} and the internal circumferential leakage flow Q_{iLr}. As shown in Figure 8, there are two contact lengths between the 2D piston and cylinder block, L_{p1} and L_{p2}, and each accounts for half of the circumference of the 2D piston. The internal axial leakage flow can be calculated using the standard leakage Equation (12) [23].

$$Q_{\mathrm{iLa}} = \frac{1}{2}\pi D\cdot[\frac{1}{12\mu L_{\mathrm{p1}}}h^3\cdot(p_{\mathrm{L}} - p_{\mathrm{R}}) - \frac{h}{2}v_{\mathrm{p}}] + \frac{1}{2}\pi D\cdot[\frac{1}{12\mu L_{\mathrm{p2}}}h^3\cdot(p_{\mathrm{L}} - p_{\mathrm{R}}) - \frac{h}{2}v_{\mathrm{p}}] \tag{12}$$

where p_{r} is the instantaneous right displacement chamber pressure.

The inter-circumferential leakage flow would occur during pump rotation, as shown in Figure 9. Since the inflow by the shear flow is equal to the outflow, the inter-circumferential leakage flow due to the shear flow is not considered. The internal circumferential leakage flow can be calculated using the standard leakage Equation (13).

$$Q_{\mathrm{iLr}} = L_{\mathrm{g}}\cdot\frac{1}{12\mu L_{\mathrm{r}}}h^3\cdot(p_{\mathrm{L}} - p_{\mathrm{R}}) \tag{13}$$

where L_{r} is the circumferential contact length between the 2D piston and cylinder block and is obtained using Equation (14).

$$L_{\mathrm{r}} = \begin{cases} 4\omega\frac{D}{2}t & 0 < t \le \frac{\pi}{4\omega} \\ 4\omega\frac{D}{2}(\frac{\pi}{2\omega} - t) & \frac{\pi}{4\omega} < t \le \frac{\pi}{2\omega} \\ 4\omega\frac{D}{2}(t - \frac{\pi}{2\omega}) & \frac{\pi}{2\omega} < t \le \frac{3\pi}{4\omega} \\ 4\omega\frac{D}{2}(\frac{\pi}{\omega} - t) & \frac{3\pi}{4\omega} < t \le \frac{\pi}{\omega} \end{cases} \tag{14}$$

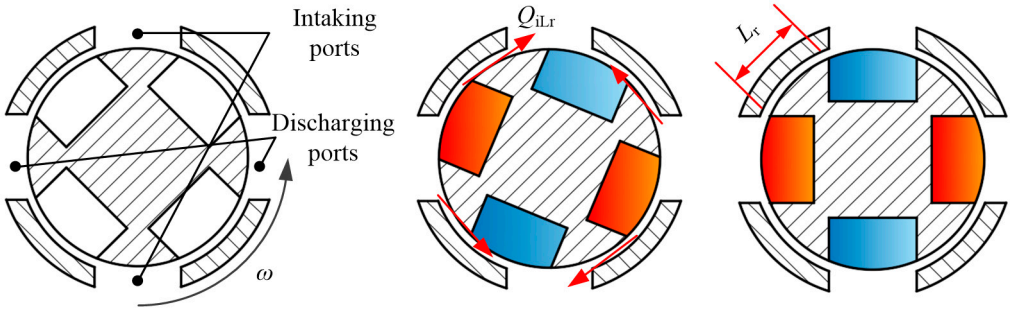


Figure 9. Cross-sections of the 2D piston and cylinder block at rotational angles of (**a**) 0 deg; (**b**) 22.5 deg; (**c**) 45 deg.

When the rotational time nears 0 or $\frac{\pi}{2\omega}$, the inter-circumferential leakage flow approaches infinity, which is inconsistent with the real situation. Under the collective effect from the ports and clearance, the face sealing for the circumferential leakage is changed to a line sealing at a specific rotational angle, as shown in Figure 9a. This line sealing might be turned into a throttle, which leads to so-called transient leakage flow and can be considered as a unique phenomenon for 2D piston pumps. Thus, Equation (13) is modified to obtain Equation (15).

$$Q_{iLr} = \begin{cases} L_g \cdot \frac{1}{12\mu L_r} h^3 \cdot (p_L - p_R) & \left| L_g \cdot \frac{1}{12\mu L_r} h^3 \cdot (p_L - p_R) \right| < \left| C_d h L_g \sqrt{\frac{2|p_L - p_R|}{\rho}} \right| \\ C_d h L_g \sqrt{\frac{2|p_L - p_R|}{\rho}} sign(p_L - p_R) & \left| L_g \cdot \frac{1}{12\mu L_r} h^3 \cdot (p_L - p_R) \right| \geq \left| C_d h L_g \sqrt{\frac{2|p_L - p_R|}{\rho}} \right| \end{cases} \quad (15)$$

Finally, as shown in Equation (16), during the left displacement chamber discharging oil, all discharging flow can be calculated by integrating the outlet flow; then, volumetric efficiency η is obtained by comparing all discharging flow with the theoretical output flow.

$$\eta = \frac{\int_0^{t_{90deg}} Q_{out}}{t_{90deg} n V_D} \quad (16)$$

where t_{90deg} is the time that the pump rotates from 0 deg to 90 deg, and V_D is the pump's displacement.

4. Simulation Results

The volumetric efficiency of the 2D piston pump with a balanced force can be calculated by solving Equations (1)–(16). According to Table 1, parameters needed by simulation are consistent with the tested pump.

Table 1. Main parameters of the simulation.

Parameter	Value	Parameter	Value
Bulk modulus of the oil β_e (MPa)	1400	2D piston diameter D (m)	2.55×10^{-2}
Rotational speed n (rpm)	3000	Port length L_g (m)	0.01
2D piston stroke L_s (m)	2.5×10^{-3}	Clearance h (m)	2×10^{-5}
Left displacement chamber maximum volume V_M (m^3)	1.54×10^{-6}	Oil dynamic viscosity μ (kg/m·s)	3.893×10^{-2}
Orifice coefficient C_d	0.62	2D piston small diameter d (m)	1.8×10^{-2}
Load pressure p_{Load} (MPa)	8	Minimum contacting length of the piston ring L_D (m)	2.5×10^{-3}
Tank pressure p_T (MPa)	0	Two contacting lengths of the 2D piston L_{p1} and L_{p2} (m)	1.75×10^{-2} 2.5×10^{-3}
Oil density ρ (kg/m^3)	850	pump's displacement V_D (m^3/r)	5.12×10^{-6}

The volumetric efficiency is affected by backflow and leakage. This paper describes their effects on volumetric efficiency in detail from the perspectives of load pressure and rotational speed.

The positive flow rate is assumed as the outflow from the left displacement chamber.

4.1. Backflow

When the left displacement chamber is connected to the discharging ports, backflow is generated due to the instantaneous left displacement chamber pressure, which is lower than the load pressure.

As shown in Figure 10, the flow peak and the duration of the backflow increase with the increase in load pressure. As the load pressure increases, the pressure difference between the instantaneous left displacement chamber pressure and load pressure increases at a rotational angle of 0 deg; thus, more flow is needed to help the left displacement chamber establish the pressure to discharge oil.

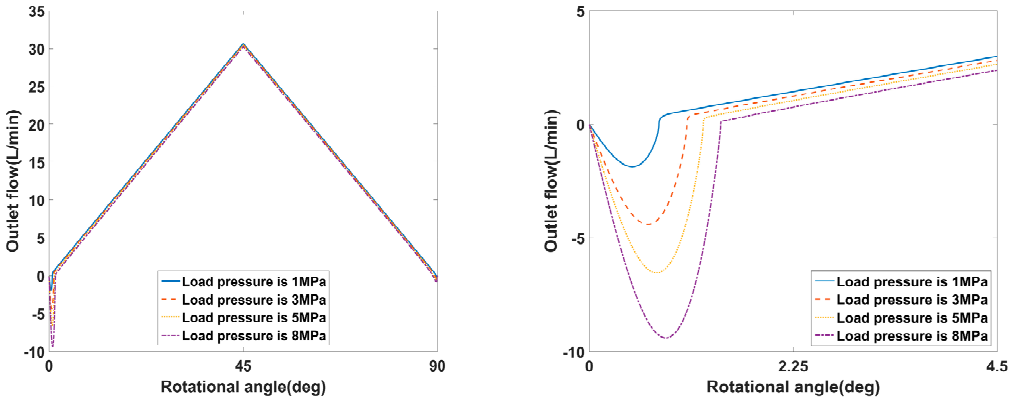


Figure 10. The outflow at load pressures 1 MPa, 3 MPa, 5 MPa, and 8 MPa for rotational angle ranges (**a**) 0–90 deg and (**b**) 0–4.5 deg.

As shown in Figure 11, the flow peak of the backflow increases with the rise in rotational speed. Due to the different rotational speeds, although the angle range of the backflow increases as the rotational speed increases, the duration of the backflow decreases. Since the load pressure is constant, the total amount of demanded backflow remains constant, and the flow peak of the backflow increases due to the decrease in the duration of the backflow.

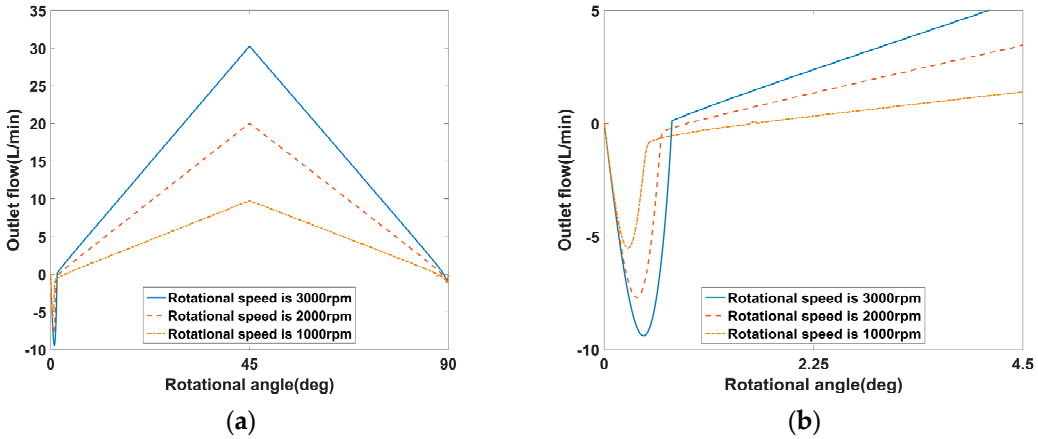


Figure 11. The outflow at rotational speeds of 1000 rpm, 2000 rpm, and 3000 rpm at angle ranges of (**a**) 0–90 deg and (**b**) 0–4.5 deg.

4.2. Leakage

The leakage of the 2D piston pump with a balanced force is composed of external leakage, internal axial leakage, and internal circumferential leakage.

As shown in Figure 12, when the left displacement chamber connects with the discharging ports, and the rotational angle nears 0 deg, the external leakage approaches 0 L/min. As the backflow helps the instantaneous left displacement chamber pressure to increase rapidly, the external leakage reaches its maximum. Then, as the contacting length and the velocity of the left piston ring increase, the external leakage decreases. When the rotational angle exceeds 45 deg, due to the decrease in the velocity of the left piston ring, the external leakage increases.

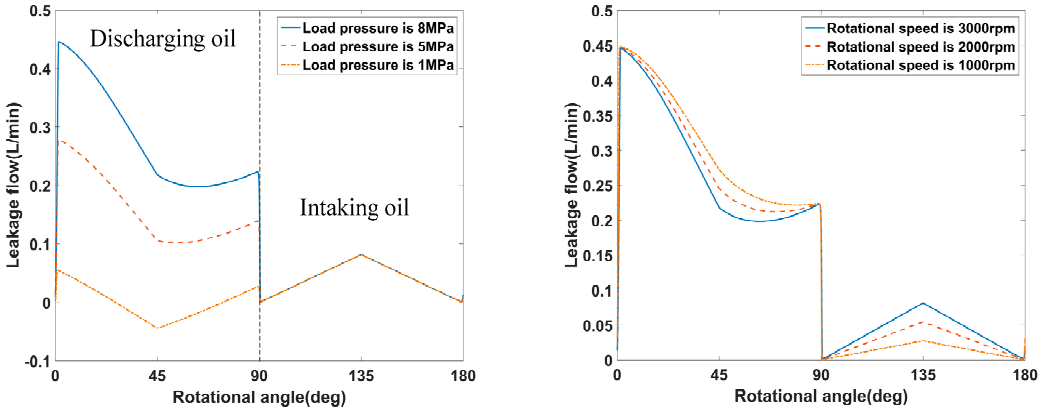


Figure 12. The external leakage at various (**a**) load pressures and (**b**) rotational speeds.

As the rotational speed decreases, the leakage from the shear flow decreases. As the directions of leakage due to the pressure difference and shear flow are opposite, the external leakage increases as the rotational speed decreases at the discharging oil.

When the load pressure is 1 MPa, the overall external leakage is negative at the discharging oil. The external leakage contributes to the volumetric efficiency of the pump at low load pressures.

As shown in Figure 13, the internal axial leakage is similar to external leakage. Because the two contacting lengths between the 2D piston and cylinder block are constant, as shown in Figure 13a, the internal axial leakage linearly declines and then rises for the rotational angle range 0–90 deg. When the load pressure is 1 MPa, the overall internal axial leakage also presents negative flow at the discharging oil.

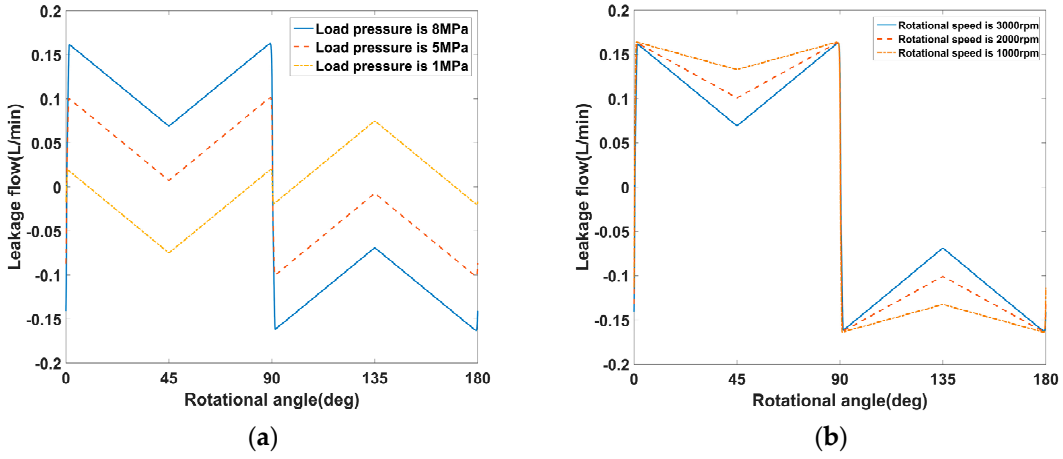


Figure 13. The internal axial leakage at various (**a**) load pressures and (**b**) rotational speeds.

As shown in Figure 14, the transient leakage of the inter-circumferential leakage is consistent with theoretical analysis and can reach 1 L/min when the rotational angle nears 0 deg or 90 deg at a load pressure of 8 MPa. As the load pressure rises, since the pressure difference between the left and right displacement chamber rises, the transient leakage increases. As the rotational speed increases, the inter-circumferential leakage is almost unchanged, except for the reduction in the reflow region.

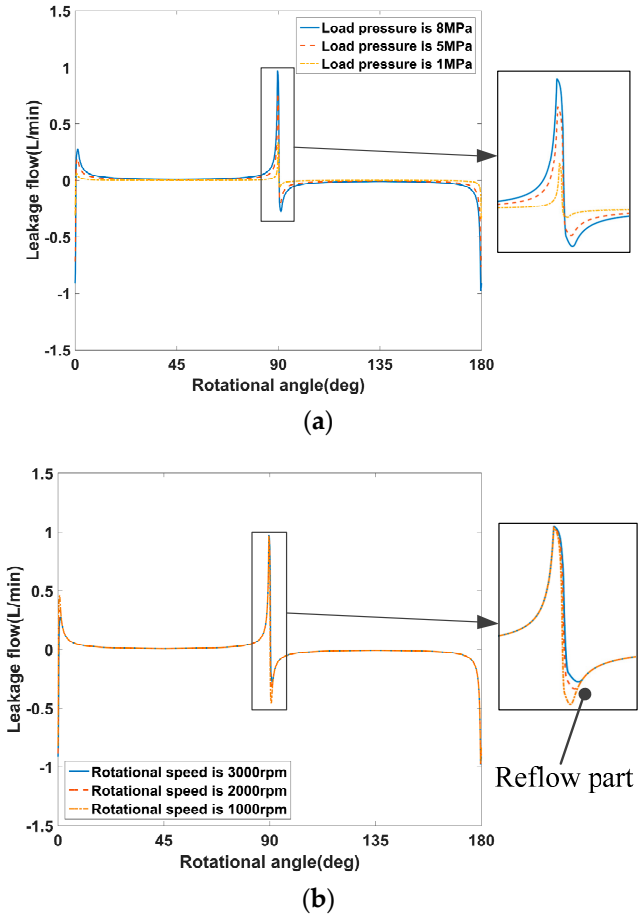
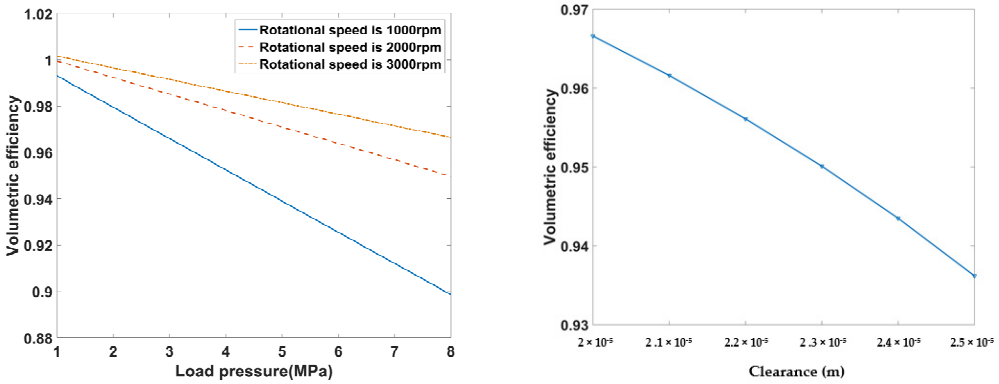


Figure 14. The inter-circumferential leakage at various (**a**) load pressures and (**b**) rotational speeds.

4.3. Volumetric Efficiency

As shown in Figure 15a, the simulated volumetric efficiency distribution of the 2D piston pump with a balanced force is consistent with the above analysis. With the load pressure rising, since the backflow and the leakage increase, the volumetric efficiency decreases. Furthermore, as the rotational speed increases, the volumetric efficiency increases because the increased velocity of the backflow and leakage is lower than the increased velocity of the outlet flow.



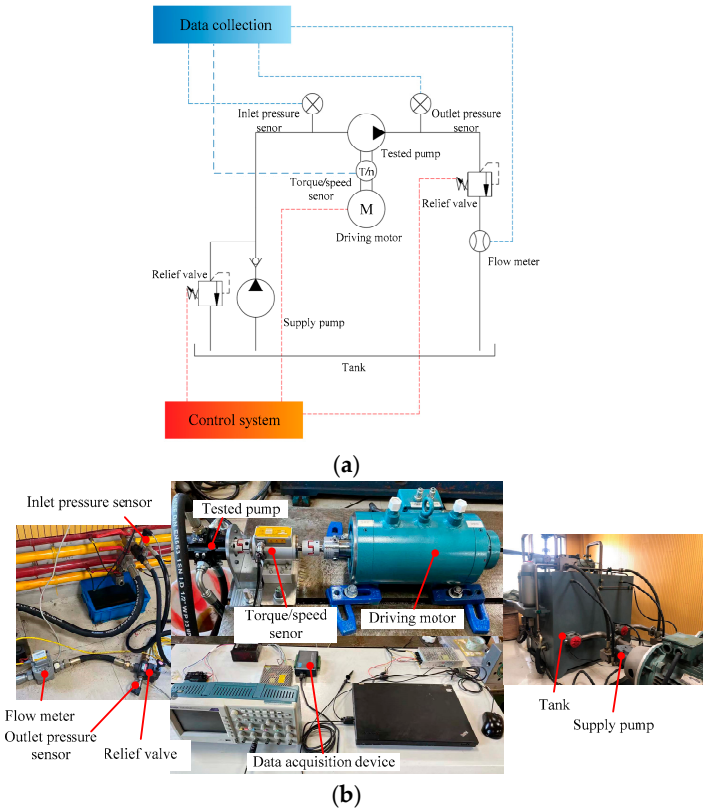
(**a**) (**b**)

Figure 15. Simulation results of volumetric efficiency distribution at various (**a**) rotational speeds and load pressures and (**b**) clearances.

In addition, due to wear and manufacturing accuracy, clearances between the piston rings, 2D piston, and cylinder block are easily changed. As shown in Figure 15b, the volumetric efficiency decreases significantly with the increase of the clearance.

5. Experimental Results

As shown in Figure 16a, the test rig consists of a tested pump, a torque sensor, a driving motor, a supply pump, a tank, two pressure sensors installed at the inlet and the outlet of the tested pump, a relief valve, a flow meter, and a data acquisition device. The tested pump and driving motor are connected by a flexible coupling, which increases the stability of the transmission chain at high rotational speeds. To prevent cavitation, the inlet pressure is added to 0.5 MPa by the supply pump. The accuracies of the related sensors are shown in Table 2.



(**a**)

(**b**)

Figure 16. The test rig. (**a**) schematic of the test rig, and (**b**) overview of the test rig.

Table 2. The details of the related sensors.

Description	Accuracy
Flow meter	Range 0–100 L/min, accuracy ± 0.1%
Torque/speed sensor	Range 0–10 Nm, accuracy ± 0.1%, rotational speed range 0–18,000 rpm
Pressure sensor	Range 0–100 bar, accuracy ± 0.3%

The load pressure-flow characteristic data of the tested pump are measured through fixing the speed of the driving motor and adjusting the relief valve installed at the outlet of the tested pump to control the load pressure. The load pressures, rotational speeds, and outlet flow are recorded, as shown in Table 3.

Table 3. The tested data of the load pressure-flow characteristic.

Rotational Speed	Outlet Flow (L/min)							
(r/min)	1 MPa	2 MPa	3 MPa	4 MPa	5 MPa	6 MPsa	7 MPa	8 MPa
1000	5.0	4.8	4.7	4.6	4.5	4.4	4.3	4.2
2000	10.0	9.8	9.7	9.5	9.3	9.3	9.1	9.0
3000	15.2	15.0	14.8	14.6	14.4	14.3	14.1	13.9

On the other hand, the range and accuracy of the flowmeter are too large to accurately measure the output flow, and only one decimal place can be taken. The tested data of rotational speeds 1000 rpm and 3000 rpm are compared with the corresponding simulations, respectively, as shown in Figure 17.

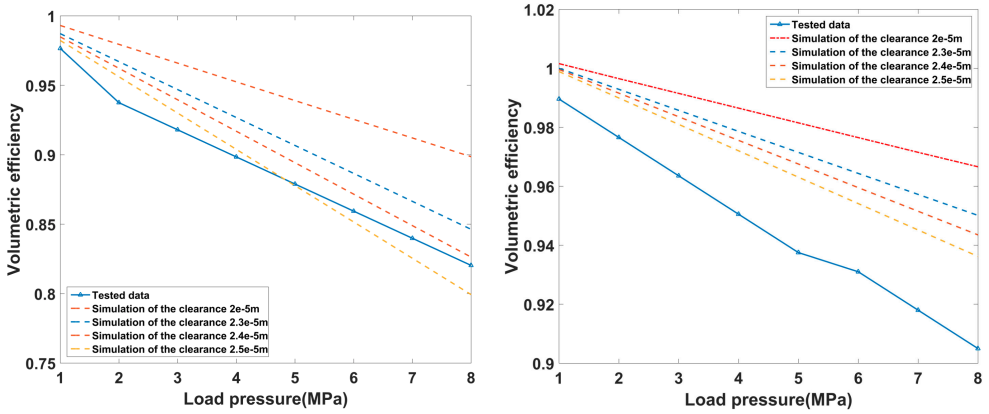


Figure 17. Volumetric efficiency distributions of the tested data and simulations at rotational speeds (**a**) 1000 rpm and (**b**) 3000 rpm.

Although high-precision machining is used to ensure the size of the clearance designed to be 2×10^{-5} m during the machining process, errors still remain in the clearance because of the inevitable machining errors and wear. However, it is regrettable that this clearance cannot be accurately measured due to the lack of corresponding detection equipment. To improve the match between the simulation and experiment, the maximum clearance 2.5×10^{-5} m and the minimum clearance 2×10^{-5} m are considered. As shown in Figure 17a, when the clearance changes from 2×10^{-5} m to 2.5×10^{-5} m, the simulations are closer to the tested data, and the trends of the tested data and simulations linearly decline at a rotational speed of 1000 rpm. Especially when the size of the clearance is 2.4×10^{-5} or 2.5×10^{-5} m, the maximum numerical difference between simulation and experimental data does not exceed 3%. However, when the rotational speed is 3000 rpm, a numerical difference remains between the volumetric efficiencies of the tested data and simulations and increases as the load pressure rises. There are three explanations for this difference.

Firstly, during discharging the oil, the leakage due to the shear flow no longer contributes to volumetric efficiency and is not consistent with the standard leakage equation at a high rotational speed.

Secondly, as other studies have shown, the friction and churning losses in the pump exacerbate the increase in oil temperature and reduce the oil viscosity at high rotational speeds, resulting in leakage increase.

Thirdly, when the rotational speed increases, the 2D piston may be eccentric in the cylinder block, which causes an increase in leakage.

Fourthly, because of the lack of equipment for detecting the clearance and the inaccuracy of test methods and test equipment, the experimental data and simulation have deviated.

6. Conclusions

In this paper, a new 2D piston pump with a balanced force is proposed, and its volumetric efficiency is studied through mathematical modeling. The volumetric losses generated by the backflow and leakage are analyzed from the perspectives of load pressure and rotational speed. A test bench is built to measure the volumetric efficiency of the tested pump and compared to the mathematical model. According to the experimental results, the following conclusions can be drawn:

Firstly, the mathematical model is consistent with the experimental data, and as the load pressure increases, the volumetric efficiency linearly decreases at various rotational speeds.

Secondly, because the rotational speed has little effect on the leakage and hardly affects the total amount of the backflow, increasing rotational speed is beneficial to increasing volumetric efficiency. However, the increase in the rotational speed affects the flow ripple, which requires further investigation.

Thirdly, the tested data and simulations differ when the rotational speed is 3000 rpm, and the difference increases as the load pressure rises. Leakage is the main reason for this difference. When the rotational speed increases, the standard leakage equation is no longer applicable, and the increase in the oil temperature causes the viscosity to decrease, and the eccentricity of the 2D piston in the cylinder block causes the leakage to increase.

Future research on volumetric efficiency will concern the pump temperature field and the viscosity-temperature equation. The gap flow and the effect of clearance on the volumetric efficiency in 2D pumps need to be studied in more detail. Finally, the rotational speed of the 2D piston pump with a balanced force needs to be further increased.

Author Contributions: Formal analysis, S.L.; data curation, Y.C.; writing—original draft preparation, Y.H.; writing—review and editing, C.D.; funding acquisition, J.R. All authors have read and agreed to the published version of the manuscript.

Funding: This research was funded by the National Key Research and Development Program of China, grant number 2019YFB2005201, by the National Natural Science Foundation of China, grant numbers 51675482 and 51805480.

Conflicts of Interest: The authors declare no conflict of interest.

References

1. Habibi, S.; Goldenberg, A. Design of a new high-performance electrohydraulic actuator. *IEEE ASME Trans. Mechatron.* **2000**, *5*, 158–164. [CrossRef]
2. Yang, H.Y.; Pan, M. Engineering research in fluid power: A review. *J. Zhejiang Univ. Sci. A* **2015**, *16*, 427–442. [CrossRef]
3. Xu, B.; Ding, R.G.; Zhang, J.H. Experiment research on individual metering systems of mobile machinery based on coordinate control of pump and valves. *J. Zhejiang Univ. (Eng. Sci.)* **2015**, *49*, 93–101.
4. Alle, N.; Hiremath, S.S.; Makaram, S.; Subramaniam, K.; Talukdar, A. Review on electro hydrostatic actuator for flight control. *Int. J. Fluid Power* **2016**, *17*, 125–145. [CrossRef]
5. Chao, Q.; Zhang, J.; Xu, B.; Huang, H.; Pan, M. A review of high-speed electro-hydrostatic actuator pumps in aerospace applications: Challenges and solutions. *J. Mech. Des.* **2019**, *141*, 050801. [CrossRef]

6. Manring, N.D.; Mehta, V.S.; Nelson, B.E.; Graf, K.J.; Kuehn, J.L. Increasing the Power Density for Axial-Piston Swash-Plate Type Hydrostatic Machines. *J. Mech. Des.* **2013**, *135*, 071002. [CrossRef]
7. Crowder, R.M. Electrically powered actuation for civil aircraft. In Proceedings of the IEE Colloquium on Actuator Technology: Current Practice and New Developments, London, UK, 10 May 1996.
8. Wu, S.; Yu, B.; Jiao, Z.; Shang, Y.; Luk, P.C.K. Preliminary design and multi-objective optimization of electro-hydrostatic actuator. *Proc. Inst. Mech. Eng. Part G J. Aerosp. Eng.* **2017**, *231*, 1258–1268. [CrossRef]
9. Manring, N.D.; Mehta, V.S.; Nelson, B.E.; Graf, K.J.; Kuehn, J.L. Scaling the Speed Limitations for Axial-Piston Swash-Plate Type Hydrostatic Machines. *J. Dyn. Syst. Meas. Control* **2014**, *136*, 031004. [CrossRef]
10. Manring, N.D. Friction forces within the cylinder bores of swash-plate type axial-piston pumps and motors. *J. Dyn. Syst. Meas. Control* **1999**, *121*, 531–537. [CrossRef]
11. Schenk, A.; Ivantysynova, M. An investigation of the impact of elastohydrodynamic deformation on power loss in the slipper swashplate interface. In Proceedings of the 8th JFPS International Symposium on Fluid Power, Okinawa, Japan, 25–28 October 2011; pp. 228–234.
12. Manring, N.D. Tipping the cylinder block of an axial-piston swash-plate type hydrostatic machine. *J. Dyn. Syst. Meas. Control* **2000**, *122*, 216–221. [CrossRef]
13. Zhang, J.; Chao, Q.; Xu, B.; Pan, M.; Wang, Q.; Chen, Y. Novel three-piston pump design for a slipper test rig. *Appl. Math. Model.* **2017**, *52*, 65–81. [CrossRef]
14. Zhang, J.H.; Chen, Y.; Xu, B.; Pan, M.; Chao, Q. Effects of splined shaft bending rigidity on cylinder tilt behaviour for high-speed electro-hydrostatic actuator pumps. *Chin. J. Aeronaut.* **2019**, *32*, 499–512. [CrossRef]
15. Strmčnik, E.; Majdič, F.; Kalin, M. Water-lubricated behaviour of AISI 440C stainless steel and a DLC coating for an orbital hydraulic motor application. *Tribol. Int.* **2019**, *131*, 128–136. [CrossRef]
16. Shang, L.; Ivantysynova, M. Port and case flow temperature prediction for axial piston machines. *Int. J. Fluid Power* **2015**, *16*, 35–51.
17. Zecchi, M.; Mehdizadeh, A.; Ivantysynova, M. A novel approach to predict the steady state temperature in ports and case of swash plate type axial piston machines. In Proceedings of the 13th Scandinavian International Conference on Fluid Power, Linköping, Sweden, 3–5 June 2013; pp. 177–187.
18. Huang, Y.; Ding, C.; Wang, H.; Ruan, J. Numerical and experimental study on the churning losses of 2D high-speed piston pumps. *Eng. Appl. Comput. Fluid Mech.* **2020**, *14*, 764–777. [CrossRef]
19. Zhang, J.H.; Li, Y.; Xu, B.; Chen, X.; Pan, M. Churning losses analysis on the thermal-hydraulic model of a high-speed electro-hydrostatic actuator pump. *Int. J. Heat Mass Transf.* **2018**, *127*, 1023–1030. [CrossRef]
20. Zhang, J.H.; Li, Y.; Xu, B.; Pan, M.; Lv, F. Experimental Study on the Influence of the Rotating Cylinder Block and Pistons on Churning Losses in Axial Piston Pumps. *Energies* **2017**, *10*, 662. [CrossRef]
21. Ruan, J.; Burton, R.; Ukrainetz, P.; Xu, Y.M. Two-dimensional pressure control valve. *Proc. Inst. Mech. Eng. Part C J. Mech. Eng. Sci.* **2001**, *215*, 1031–1038. [CrossRef]
22. Ding, C.; Zhu, Y.H.; Liu, L.; Tong, C.W.; Ruan, J. Research on a Novel Flowmeter With Parallel Two-Dimensional Pistons as Its Metering Units. *IEEE Access* **2019**, *7*, 110912–110927. [CrossRef]
23. Shentu, S.; Ruan, J.; Qian, J.; Meng, B.; Wang, L.; Guo, S. Study of flow ripple characteristics in an innovative two-dimensional fuel piston pump. *J. Braz. Soc. Mech. Sci. Eng.* **2019**, *41*, 464. [CrossRef]
24. Jin, D.C.; Ruan, J.; Li, S.; Meng, B.; Wang, L.F. Modelling and validation of a roller-cam rail mechanism used in a 2D piston pump. *J. Zhejiang Univ. Sci. A* **2019**, *20*, 201–217. [CrossRef]
25. Xing, T.; Xu, Y.; Ruan, J. Two-dimensional Piston Pump: Principle, Design, and Testing for Aviation Fuel Pumps. *Chin. J. Aeronaut.* **2019**, *33*, 1349–1360. [CrossRef]
26. Huang, Y.; Ruan, J.; Zhang, C.; Ding, C.; Li, S. Research on the Mechanical Efficiency of High-Speed 2D Piston Pumps. *Processes* **2020**, *8*, 853. [CrossRef]



© 2020 by the authors. Licensee MDPI, Basel, Switzerland. This article is an open access article distributed under the terms and conditions of the Creative Commons Attribution (CC BY) license (http://creativecommons.org/licenses/by/4.0/).